DIFFRACTION OF SHORT-CRESTED WAVES AROUND A CIRCULAR CYLINDER

SONGPING ZHU

Department of Mathematics, The University of Wollongong, Wollongong, NSW 2500, Australia

Abstract—In this paper, an exact solution for the diffraction of short-crested waves incident on a circular cylinder is presented. The pressure distribution and water run-up on the cylinder was found to be quite different from those of plane incident waves. The total force exerted on the cylinder in the direction of the wave propagation was found to be smaller compared to that induced by plane waves with the same wave number in the direction of the wave propagation. The total wave load increases as the wave number in the direction perpendicular to the direction of the wave propagation increases, or as the incident waves become shorter. These results show that if the wave loading is calculated, as a design criterion, according to plane incident waves, it will be over-estimated when the incident waves are short-crested. However, from the safety point of view, the wave loading formula derived from a plane incident wave may still serve as a good engineering design criterion.

1. INTRODUCTION

A COMMON problem in offshore engineering is to calculate the wave loading exerted on a circular cylinder. Wave loads on a large vertical cylinder resting on the ocean floor and piercing the water surface are evaluated by the formula proposed by MacCamy and Fuchs (1954), who found an analytical solution for linear plane waves being diffracted around a large vertical cylinder. Their results have been verified with experiments by many experimentalists (e.g. Chakrabarti and Tam, 1975; Neelamani *et al.*, 1989) and have also been utlized to verify numerical models (e.g. Tsay *et al.*, 1989; Bettess and Zienkiewicz, 1976). The experimental results have shown good agreements between the theory and the experiments for $0.2 < ka < 0.65$ (k is the wave number of the incident waves and a is the radius of the cylinder).

However, waves generated by winds blowing over the water surface in real oceans are short-crested. Short-crested waves are the waves of finite lateral extent; they have many different properties compared to a long-crested plane wave. The theory of short-crested waves was developed by Jeffreys (1924) and extended considerably by Fuchs (1952). Short-crested waves have attracted much research exploring their kinematic and dynamic properties (e.g. Roberts, 1982; Hsu *et al.*, 1979). However, no-one seems to have discussed, to the author's knowledge, the impact of the short-crested waves on a cylinder. When the incident waves are short-crested, one can conjecture that the induced pressure distribution around the cylinder will be different from that induced by plane waves. It is not so clear, on the other hand, whether or not the total wave loads exerted on a cylinder should be different when the incident waves are short-crested, nor it is clear, even if the wave loads are indeed different from those induced by the plane waves, whether the loads exerted by short-crested waves would be larger or smaller compared to the wave loads exerted by plane waves. These questions are

of significant importance to ocean engineering because the current design criterion may have to be reviewed.

In this paper, an analytical solution for the diffraction of short-crested waves around a vertical cylinder resting on the ocean floor and piercing the free surface is presented and the above questions will be addressed as a natural consequence of the results obtained from the solution.

2. FORMULATION OF THE PROBLEM

Consider that a train of monochromatic short-crested waves of frequency, ω, are propagating in the direction of the positive x-axis in an ocean with uniform depth, d, and a fixed, vertical cylinder of radius, a, is placed on the floor of the ocean as shown in Fig. 1. With the origin being placed at the center of the cylinder on the mean surface level (MSL), a cylindrical coordinate system is adopted with its z-axis pointing upward. It is assumed that the fluid is incompressible and the flow is irrotational. Therefore, there exists a velocity potential function ϕ such that the velocity components in the radial, azimuthal and vertical directions, v_r, v_θ and v_z can be expressed in terms of ϕ as

$$v_r = \frac{\partial \phi}{\partial r}, \quad v_\theta = \frac{1}{r}\frac{\partial \phi}{\partial \theta}, \quad v_z = \frac{\partial \phi}{\partial z} ,\tag{1}$$

and ϕ satisfies the Laplace equation

$$\Delta\phi = \frac{\partial^2 \phi}{\partial r^2} + \frac{1}{r}\frac{\partial \phi}{\partial r} + \frac{1}{r}\frac{\partial^2 \phi}{\partial \theta^2} + \frac{\partial^2 \phi}{\partial z^2} = 0 ,\tag{2}$$

subject to the boundary conditions

$$\frac{\partial \phi}{\partial z} = 0 \qquad\qquad \text{on } z = -d ,\tag{3}$$

$$\frac{\partial \phi}{\partial r} = 0 \qquad\qquad \text{on } r = a ,\tag{4}$$

$$\frac{\partial^2 \phi}{\partial t^2} + g\frac{\partial \phi}{\partial z} = 0 \qquad \text{on } z = 0, \quad r \ge a,\tag{5}$$

where t is the time variable and g is the gravitational acceleration.

For short-crested incident waves travelling in the positive x-direction, the velocity potential can be given by the real part of* (Fuchs, 1952)

$$\phi^{(I)} = -\frac{igA}{\omega}\frac{\cosh k(z+d)}{\cosh kd}e^{i(k_x x - \omega t)}\cos k_y y ,\tag{6}$$

in which A is the amplitude of the incident waves, $i = \sqrt{-1}$, k_x and k_y are the wave

---

* In the rest of the paper, it is implied that any physical quantity is obtained by taking the real part of the corresponding complex variable used in the solution.
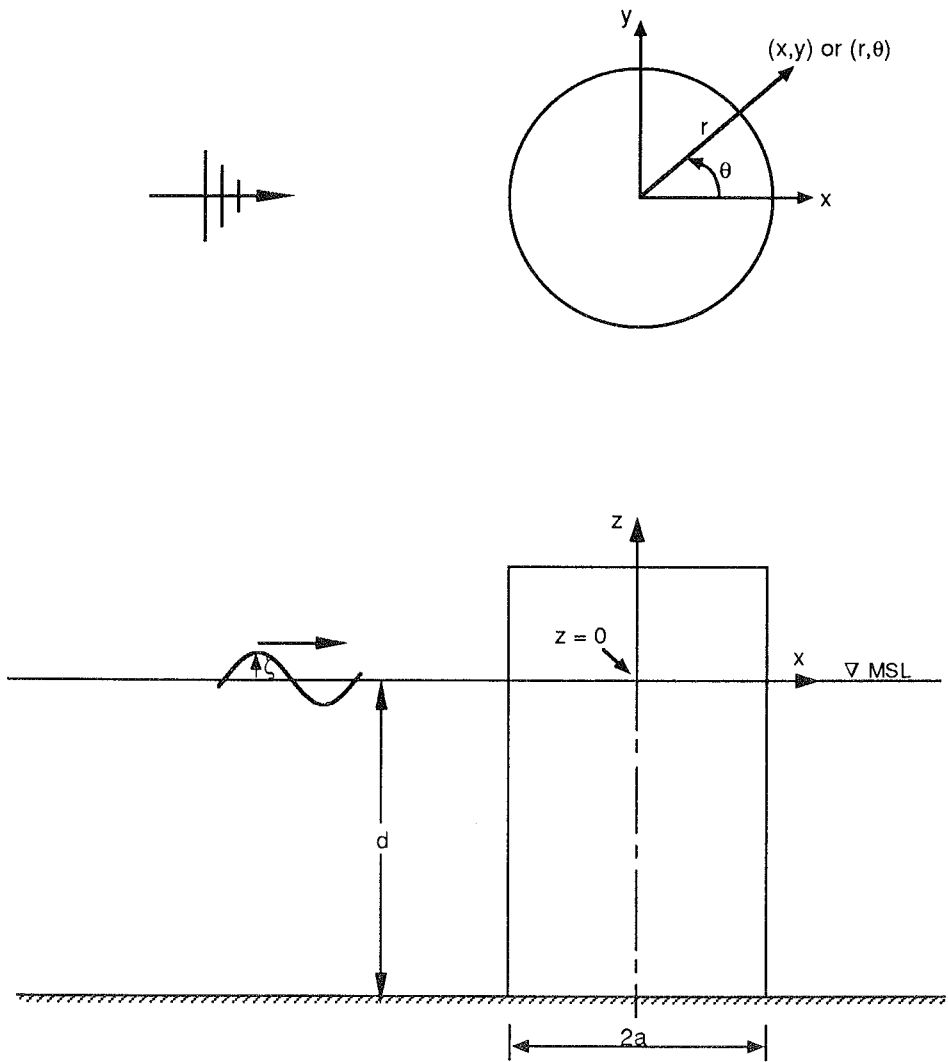
FIG. 1. A sketch for the coordinate system.

numbers in the x- and y-directions, respectively, and k is the total wave number which relates to k_x and k_y by the equation

$$k^2 = k_x^2 + k_y^2 .$$ (7)

The wave celerity with which the short-crested waves are travelling in the positive x-direction is

$$C = \left[\frac{gk}{k_x^2} \tanh kd \right]^{1/2} ,$$ (8)

which is larger than that of long-crested waves of the same wave number in the direction of the wave propagation with the same water depth. There is no wave propagating in the y-direction; the amplitude of the short-crested waves varies periodically in the direction perpendicular to the main direction of wave propagation.

The total potential now can be written as the sum of the potential of the incident waves, $\phi^{(I)}$, and the potential of scattered waves, $\phi^{(S)}$, as

$$\phi = \phi^{(I)} + \phi^{(S)} . \tag{9}$$

The governing equation and boundary conditions for the scattered waves are obtained by substituting (9) into Equations (2)–(5) as

$$\Delta\phi^{(S)} = \frac{\partial^2\phi^{(S)}}{\partial r^2} + \frac{1}{r}\frac{\partial\phi^{(S)}}{\partial r} + \frac{1}{r^2}\frac{\partial^2\phi^{(S)}}{\partial\theta^2} + \frac{\partial^2\phi^{(S)}}{\partial z^2} = 0 , \tag{10}$$

$$\frac{\partial\phi^{(S)}}{\partial z} = 0 \qquad \text{on } z = -d , \tag{11}$$

$$\frac{\partial\phi^{(S)}}{\partial r} = -\frac{\partial\phi^{(I)}}{\partial r} \qquad \text{on } r = a , \tag{12}$$

$$\frac{\partial^2\phi^{(S)}}{\partial t^2} + g\frac{\partial\phi^{(S)}}{\partial z} = 0 \qquad \text{on } z = 0 . \tag{13}$$

The scattered waves, which are the disturbances created by the presence of the cylinder, must behave as outgoing waves at infinity. Sommerfeld (1949) gave the radiation condition for the scattered waves at infinity as

$$\lim_{kr \to \infty} (kr)^{1/2}\left(\frac{\partial}{\partial r} - ik\right)\phi^{(S)} = 0 . \tag{14}$$

Equations (10)–(14) constitute the governing equation and boundary conditions for the diffraction of short-crested waves by a circular cylinder.

3. THE SOLUTION OF THE PROBLEM

In cylindrical coordinates, the incident wave potential (6) can be written as (Watson, 1962)

$$\phi^{(I)} = -\frac{igA}{\omega}\frac{\cosh k(z+d)}{\cosh kd}\left[\sum_{m=0}^{\infty} \varepsilon_m i^m J_m(k_x r)\cos m\theta\right]$$

$$\cdot \left[\sum_{n=0}^{\infty} \varepsilon_n J_{2n}(k_y r)\cos 2n\theta\right] e^{-i\omega t} , \tag{15}$$

where

$$\varepsilon_m = \begin{cases} 1 & \text{for } m = 0; \\ 2 & \text{for } m \neq 0, \end{cases} \tag{16}$$

and the J_ms are Bessel functions of mth order. To satisfy the boundary condition (5)

on the free surface, the wave number, k, and the frequency, ω, are linked by the dispersion relation

$$\omega^2 = gk \tanh kd . \tag{17}$$

After splitting the product of the two trigonometric functions, the potential of the incident waves can be written as

$$\phi^{(I)} = -\frac{igA}{2\omega} \frac{\cosh k(z+d)}{\cosh kd} \sum_{m=0}^{\infty} \sum_{n=0}^{\infty} E_m E_n i^m J_m(k_x r) J_{2n}(k_y r)$$

$$\cdot [\cos(m+2n)\theta + \cos(m-2n)\theta] e^{-i\omega t} . \tag{18}$$

The solution for the scattered waves can be constructed by first satisfying the Laplace equation and the boundary conditions (11) and (13) with two groups of infinitely many arbitrary constants as

$$\phi^{(S)} = \frac{igA}{2\omega} \frac{\cosh k(z+d)}{\cosh kd} e^{-i\omega t} \sum_{m=0}^{\infty} \sum_{n=0}^{\infty} E_m E_n i^m [A_{mn} H_{m+2n}(kr)$$

$$\cdot \cos(m+2n)\theta + B_{mn} H_{|m-2n|}(kr) \cos(m-2n)\theta] , \tag{19}$$

where $H_{m+2n}(kr)$ and $H_{|m-2n|}(kr)$ are the Hankel functions of the first kind that represent outgoing waves. Since

$$H_{m+2n}(kr) \sim \left(\frac{2}{kr}\right)^{1/2} e^{i[kr - \frac{2(m+2n)-1}{4}]\pi}, \, kr \to \infty , \tag{20}$$

and

$$H_{|m-2n|}(kr) \sim \left(\frac{2}{kr}\right)^{1/2} e^{i[kr - \frac{2|m-2n|-1}{4}]\pi}, \, kr \to \infty , \tag{21}$$

the Sommerfeld radiation condition (14) is also satisfied by (19). To determine the unknown coefficients A_{mn} and B_{mn}, the boundary condition (12) was used. With the primes denoting the differentiation of the Bessel function, $J_n(s)$, or the Hankel function, $H_n(s)$, with respect to their argument s, the coefficients A_{mn} and B_{mn} were found to be

$$A_{mn} = \frac{k_x J_m'(k_x a) J_{2n}(k_y a) + k_y J_m(k_x a) J_{2n}'(k_y a)}{k H_{m+2n}'(ka)} , \tag{22}$$

$$B_{mn} = \frac{k_x J_m'(k_x a) J_{2n}(k_y a) + k_y J_m(k_x a) J_{2n}'(k_y a)}{k H_{|m-2n|}'(ka)} . \tag{23}$$

Now, all the boundary conditions are satisfied with A_{mn} and B_{mn} being calculated from (22) and (23). Thus, all the other physical quantities such as pressure, free surface elevation, can be obtained thereafter.

4. DISCUSSION OF THE RESULTS

With the velocity potential for the scattered waves being determined, the total velocity potential can be readily written as the sum of the potential for the incident waves and the potential for the scattered waves as

$$\phi = -\frac{igA}{2\omega}\frac{\cosh k(z+d)}{\cosh kd}\, e^{-i\omega t}\sum_{m=0}^{\infty}\sum_{n=0}^{\infty}\varepsilon_m\varepsilon_n i^m Q_{mn}(r,\theta)\, , \tag{24}$$

where the function $Q_{mn}(r,\theta)$ is defined as

$$Q_{mn}(r,\theta) = [J_m(k_x r)J_{2n}(k_y r) - A_{mn}H_{m+2n}(kr)]\cos(m+2n)\theta$$
$$+ [J_m(k_x r)J_{2n}(k_y r) - B_{mn}H_{|m-2n|}(kr)]\cos(m-2n)\theta\, . \tag{25}$$

The total free-surface displacement is then given by

$$\eta = -\frac{A}{2}\, e^{-i\omega t}\sum_{m=0}^{\infty}\sum_{n=0}^{\infty}\varepsilon_m\varepsilon_n i^m Q_{mn}(r,\theta)\, . \tag{26}$$

The total force, per unit length in the direction of wave propagation, is

$$\frac{dF_z}{dz} = -a\int_0^{2\pi} p(a,\theta,z)\cos\theta\, d\theta\, , \tag{27}$$

in which $p(a,\theta,z)$ is the pressure at any point on the surface of the cylinder and is given by

$$p(a,\theta,z) = \frac{\rho gA}{2}\frac{\cosh k(z+d)}{\cosh kd}\, e^{-i\omega t}\sum_{m=0}^{\infty}\sum_{n=0}^{\infty}\varepsilon_m\varepsilon_n i^m Q_{mn}(a,\theta)\, . \tag{28}$$

By the orthogonality of cosines, the final expression of $\dfrac{dF_z}{dz}$ consists of a single term, which was obtained from the first term in $Q_{mn}(a,\theta)$ with $m = 1$, and $n = 0$, and a single summation resulted from the second term in $Q_{mn}(a,\theta)$ with $m = 2n+1$ and $m = 2n-1$,

$$\frac{dF_z}{dz} = -2\pi\rho gaA\frac{\cosh k(z+d)}{\cosh kd}\, e^{-i\omega t} R(k_x, k_y, k, a)\, , \tag{29}$$

where

$$R(k_x, k_y, k, a) = i\left[R_0(k_x, k_y, k, a) + \sum_{n=1}^{\infty} R_n(k_x, k_y, k, a)\right]\, , \tag{30}$$

and

$$R_0(k_x, k_y, k, a) = J_1(k_x a)J_0(k_y a) - \frac{k_x J_1'(k_x a)J_0(k_y a) + k_y J_1(k_x a)J_0'(k_y a)}{k\, H_1'(ka)}$$
$$H_1(ka)\, , \tag{31}$$

$$R_n(k_x, k_y, k, a) = i^{2n}\{[J_{2n+1}(k_x a)J_{2n}(k_y a) - B_{2n+1,n}H_1(ka)]$$
$$- [J_{2n-1}(k_x a)J_{2n}(k_y a) - B_{2n-1,n}H_1(ka)]\} \ . \tag{32}$$

The function $R(k_x, k_y, k, a)$ determines the water run-up and the pressure distribution around the cylinder. It also determines the first-order total horizontal force on the cylinder, F_x, which can be readily found by integrating (29) with respect to z,

$$F_z = \int_{-d}^0 \frac{\mathrm{d}F_z}{\mathrm{d}z} \, \mathrm{d}z = - 2\pi\rho g A a d \, \frac{\tanh kd}{kd} \, \mathrm{e}^{-i\omega t} R(k_x, k_y, k, a) \ , \tag{33}$$

and the total moment about an axis parallel to the y-axis passing through the bottom of the cylinder,

$$M_y = \int_{-d}^0 (z+d) \frac{\mathrm{d}F_z}{\mathrm{d}z} \, \mathrm{d}z = - 2\pi\rho g A a d^2 \, \mathrm{e}^{-i\omega t} R(k_x, k_y, k, a)$$
$$\frac{kd \sinh kd - \cosh kd + 1}{(kd)^2 \cosh kd} \ . \tag{34}$$

Therefore, only the function $R(k_x, k_y, k, a)$ needs to be discussed. Other important physical quantities such as F_x and M_y are obtained by multiplying the function $R(k_x, k_y, k, a)$ with some constants given in the expressions (33) and (34).

For a plane wave with wave number k, the total velocity potential given in (24) as well as other quantities obtained here reduce to the results obtained by MacCamy and Fuchs (1954) after letting $k_x \rightarrow k$ and $k_y \rightarrow 0$. Therefore, the diffraction problem with plane incident waves can be regarded as a limiting case for the problem presented here.

Following Mei (1989), the inertia coefficient, C_M, and drag coefficient, C_D, per unit height can also be derived; they are generally functions of k_x and k_y (their expressions are lengthy and so are included in the Appendix). It is very interesting that both of these coefficients were found, through numerical calculations, to be invariants if the product of the total wave number, k, and the radius of the cylinder, a, are kept as a constant. Although no analytical proof has been obtained at this stage, many numerical calculations with different combinations of k_x and k_y have been carried out to show that the inertia coefficient, C_M, and drag coefficient, C_D, per unit height are indeed the invariants of ka. Here, we chose, among other numerical results obtained, Figs 2 and 3, in which the variation of C_M and C_D are plotted against the variation of k_y/k_x, for k being taken with four different values, respectively, but ka being kept as a constant. As can be clearly seen, four curves coincide with each other. However, since the total force per unit height can be expressed as

$$\frac{\mathrm{d}F_z}{\mathrm{d}z} = \pi k_x a^2 \sqrt{C_M^2 + C_D^2} \ , \tag{35}$$

the total force changes with the variation of k_x; it varies linearly with the wave number in the direction of the wave propagation, k_x. Some special cases have been considered and the numerical results for the total forces exerted on the cylinder are listed in Table 1. This can be seen also in Fig. 4, in which the total force factor, $2\pi a R(k_x, k_y, k, a)$, is plotted against the ratio of k_y/k_x for fixed k and a.
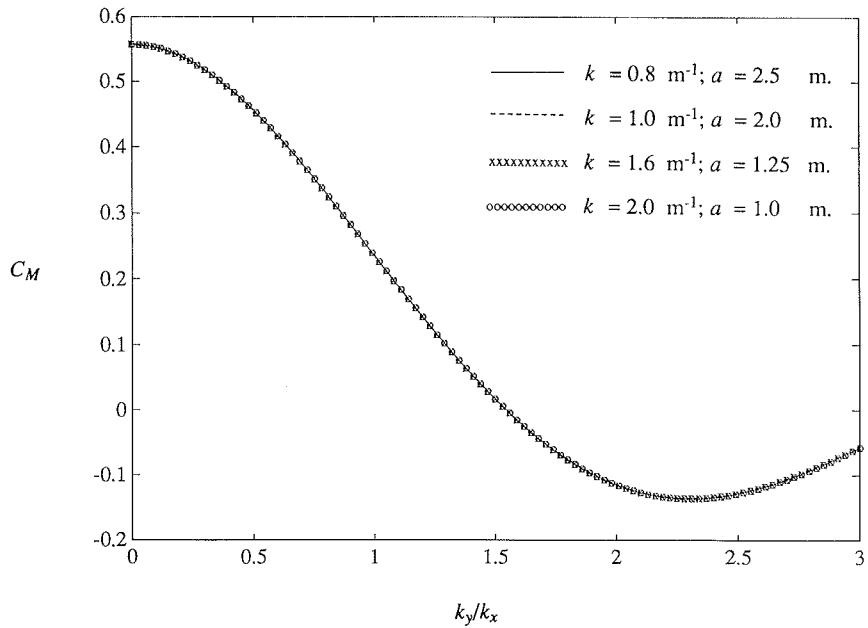
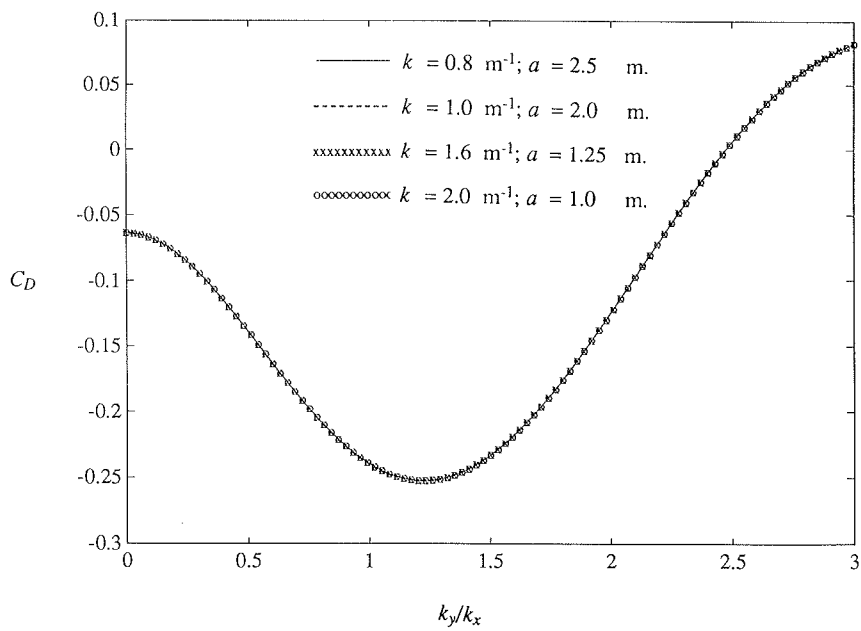FIG. 2. The variation of the inertia coefficient, C_M, vs the ratio k_y/k_x.

FIG. 3. The variation of the drag coefficient, C_D, vs the ratio k_y/k_x.

TABLE 1. THE INERTIA, DRAG COEFFICIENTS AND TOTAL FORCES

Cases	k_x (1/m)	k_y (1/m)	k (1/m)	a (m)	C_M	C_D	$\|2\pi a R(k_x, k_y, k, a)\|$ (m)
1	1.0	1.0	$\sqrt{2}$	1.0	0.8824	0.2271	2.1421
2	$\sqrt{0.56}$	1.2	$\sqrt{2}$	1.0	0.8824	0.2271	2.8626
3	1.2	$\sqrt{0.56}$	$\sqrt{2}$	1.0	0.8824	0.2271	3.4351
4	$\sqrt{2}$	0.0	$\sqrt{2}$	1.0	0.8824	0.2271	4.0483
5	1.0	1.0	$\sqrt{2}$	2.0	0.8824	−0.2398	3.1601
6	$\sqrt{0.56}$	1.2	$\sqrt{2}$	2.0	0.8824	−0.2398	4.2228
7	1.2	$\sqrt{0.56}$	$\sqrt{2}$	2.0	0.8824	−0.2398	5.0674
8	$\sqrt{2}$	0.0	$\sqrt{2}$	2.0	0.8824	−0.2398	5.9720
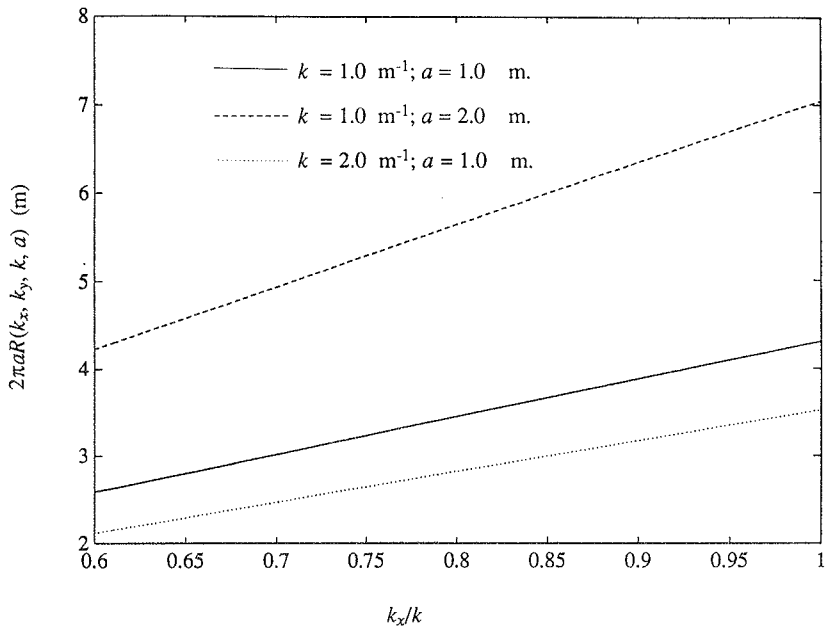
FIG. 4. The variation of the total force vs the ratio of k_x/k for fixed k and a.

For a fixed wave number, k_x, as the wave length in the direction perpendicular to the wave propagation decreases, that is, as the waves become shorter and shorter, the total force exerted on the cylinder becomes smaller and smaller. This can be observed in Fig. 5, in which the total force is plotted against the ratio k_y/k_x, for k_x being held
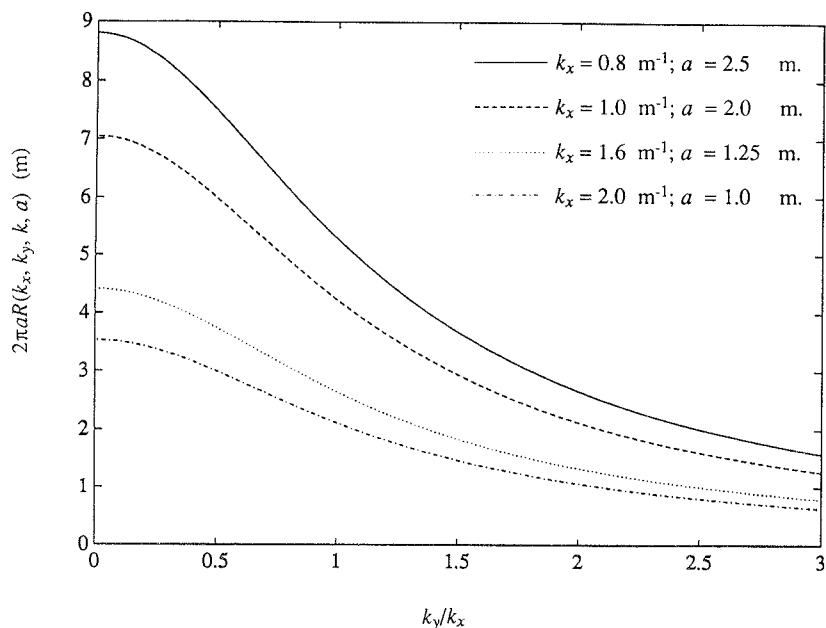
Fig. 5. The variation of the total force vs the ratio of k_y/k_x for fixed k_x and a.

as four different constants. One can therefore conclude that the maximum wave loading to a cylinder is achieved when the incident waves are plane waves. If the formula derived from the plane waves is used as a design criteria for a cylinder in a short-crested sea, it will be safe always with the wave loads being overestimated. With the wave crests being slightly shorter than that of plane waves, say for the ratio of k_y and k_x being 0.5, the wave load could drop approximately 15%.

The run-up on the cylinder is quite different when the incident waves becomes short-crested. In Fig. 6, the dimensionless water run-up, η/A, on a cylinder with radius a = 1 m is plotted against the variable θ/π for some different combinations of k_x and k_y but the same total wave number k. As one can see, for $ka = \sqrt{2}$, the waves near the front side of the cylinder, namely $\theta = \pi$, have the largest amplitude when the incident waves have infinite wavelength ($k_y = 0$) in the direction perpendicular to the wave propagation. The wave amplitude decreases here monotonically as the incident waves gradually become short-crested. For the other extreme, that is, k_x becomes zero and $k_y = k$, the amplitude of the waves on the front side of the cylinder reduced to a minimum. On the other hand, there is no such monotonic decrease of the water run-up on the lee side of the cylinder where $\theta = 0$. A minimum amplitude seems to exist between the two extremes of $k_x = k$ and $k_y = k$. The same conclusion can be drawn for a cylinder with radius $a = 2$ m as shown in Fig. 7. However, the diffraction effects become stronger compared with those of a more slender cylinder. With larger cylinders, the wave amplitude on the front side of the cylinder becomes bigger and the wave amplitude becomes smaller on the lee side with the incident waves having the same wave numbers. For larger total wave number, the pattern of the run-up for
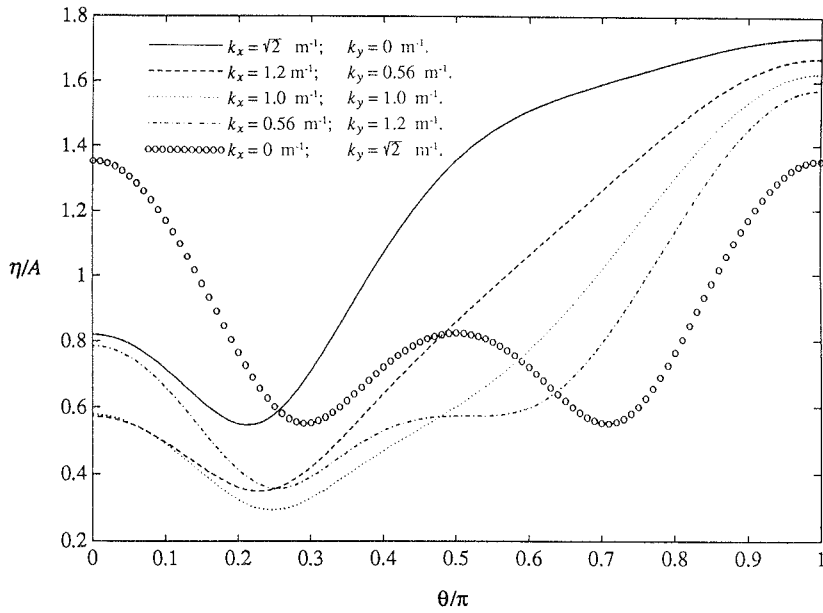
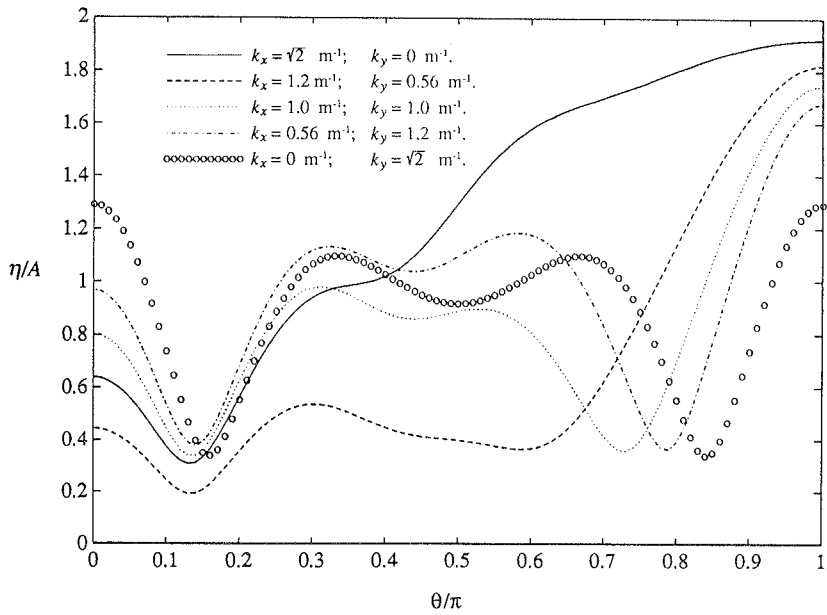FIG. 6. The water run-up of a cylinder with radius $a = 1.0$ m and total incident wave number $k = \sqrt{2}$ m^{-1}.

FIG. 7. The water run-up of a cylinder with radius $a = 2.0$ m and total incident wave number $k = \sqrt{2}$ m^{-1}.

short-crested incident waves becomes more complicated in a manner similar to that shown by Mei (1989) for plane incident waves. Nevertheless, the above observation still holds as can be seen from Figs 8 and 9, in which k is increased from $\sqrt{2}$ to $\sqrt{5}$.

The change of the water run-up is a natural consequence of the complicated wave pattern resulting from the short-crested waves impinging on a cylinder. In Figs 10–17, the co-amplitude and co-phase lines for long- and short-crested incident waves of amplitude $a = 0.01$ m diffracting around a circular cylinder with radius of 1.0 m are plotted. In all the figures, the wave number in the x-direction was fixed to 1.0 m^{-1}, whereas the wave number in the y-direction was varied from 0 to 1.0 m^{-1}, that is, from long-crested plane waves shown in Figs 10 and 11 to short-crested waves shown in Figs 12–17. The thick lines in all the co-phase plots were due to the sudden change of the phase values from $3\pi/2$ back to $-\pi/2$ when the phase angle was evaluated using the arctan function. Comparing all the co-amplitude plots, one can readily find that the amplitude of the diffracted waves in the lee region of the cylinder becomes smaller as the incident waves become shorter. The region for the large amplitude waves in front of the cylinder shrinks as well. This is expected because some parts of the incident waves are of very small amplitude; the wave energy per unit length in the y-direction for short-crested waves is smaller compared to that of long-crested plane waves. It is, however, very interesting to note that as wave crests became short, amphidromic points formed in the co-phase plots (see Figs 13, 15 and 17). These amphidromic points were closer to each other as the wave crests became shorter. The phases near two adjacent amphidromic points rotate from $-\pi/2$ to $3\pi/2$ clockwise and counter-clockwise around the amphidromic points, respectively. The wave pattern becomes more complex as the
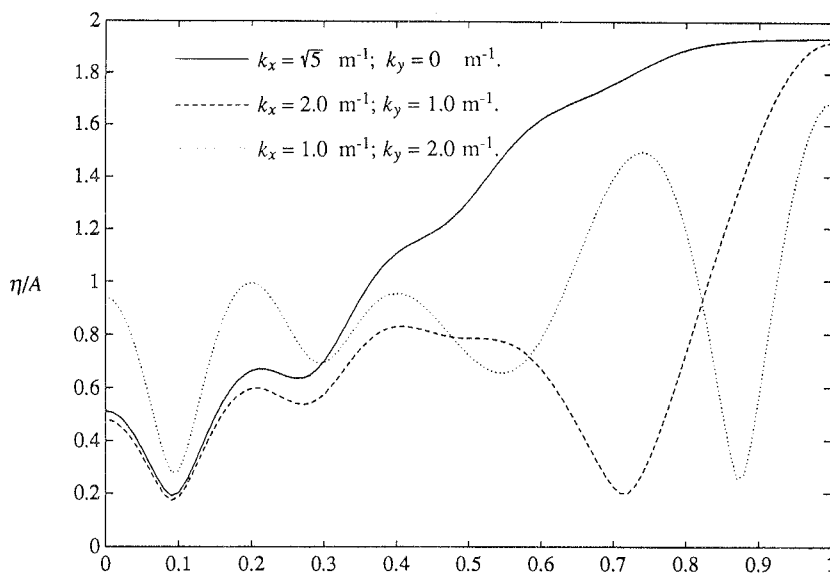

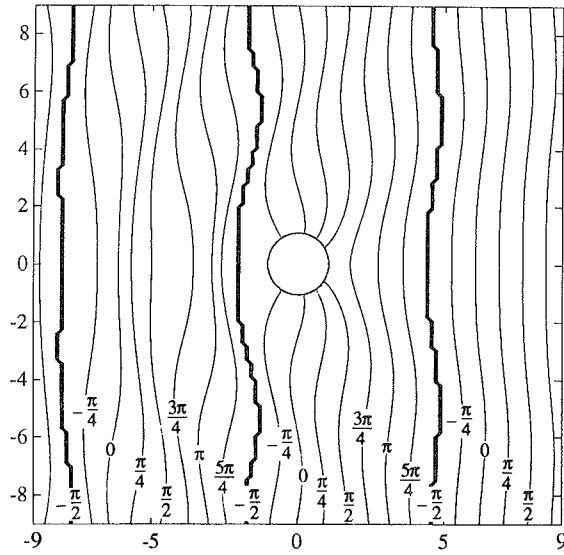FIG. 8. The water run-up of a cylinder with radius $a = 1.0$ m and total incident wave number $k = \sqrt{5}$ m^{-1}.

FIG. 9. The water run-up of a cylinder with radius $a = 2.0$ m and total incident wave number $k = \sqrt{5}$ m^{-1}.
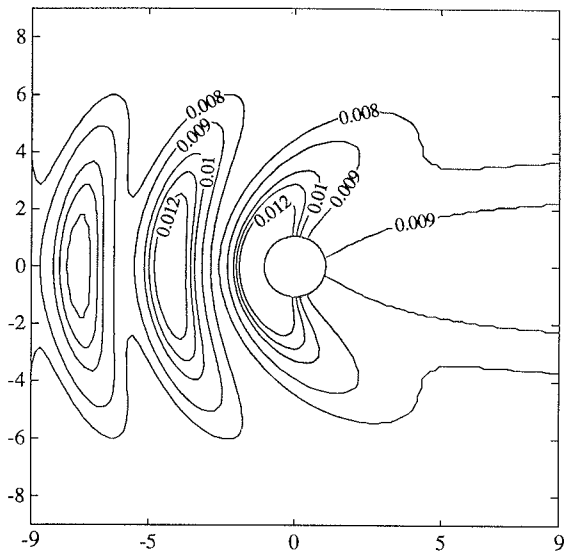

FIG. 10. The curves of equal amplitude (co-amplitude with units in meters) for the incident waves with longitudinal and lateral wave numbers $k_x = 1.0$ m^{-1} and $k_y = 0.0$ m^{-1}, respectively.
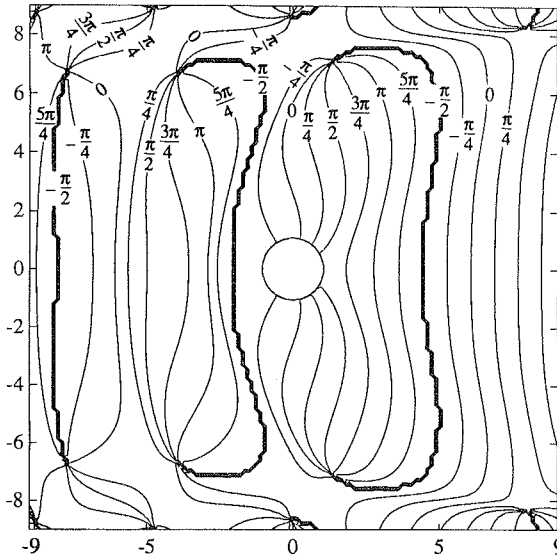
FIG. 11. The curves of equal phase (co-phase) for the incident waves with longitudinal and lateral wave numbers $k_x = 1.0$ m^{-1} and $k_y = 0.0$ m^{-1}, respectively.
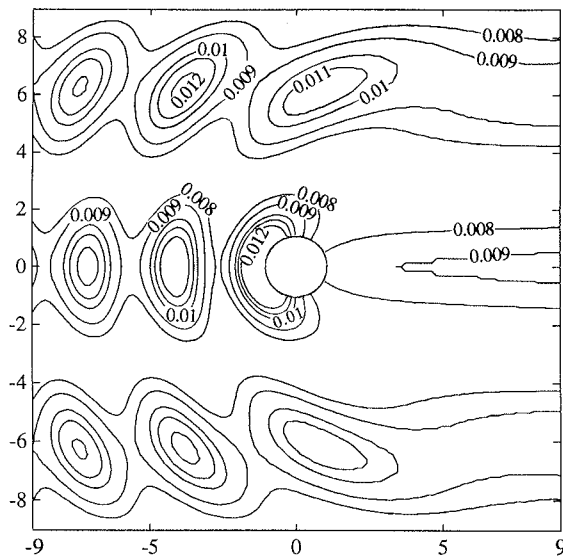

FIG. 12. The curves of equal amplitude (co-amplitude with units in meters) for the incident waves with longitudinal and lateral wave numbers $k_x = 1.0$ m^{-1} and $k_y = 0.2$ m^{-1}, respectively.
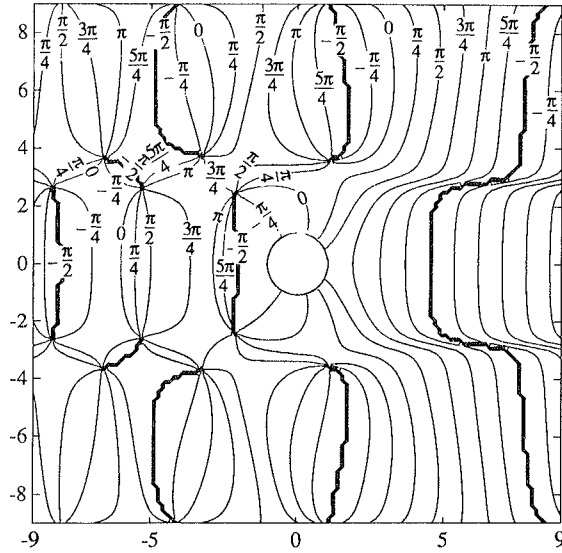
FIG. 13. The curves of equal phase (co-phase) for the incident waves with longitudinal and lateral wave numbers $k_x = 1.0$ m^{-1} and $k_y = 0.2$ m^{-1}, respectively.
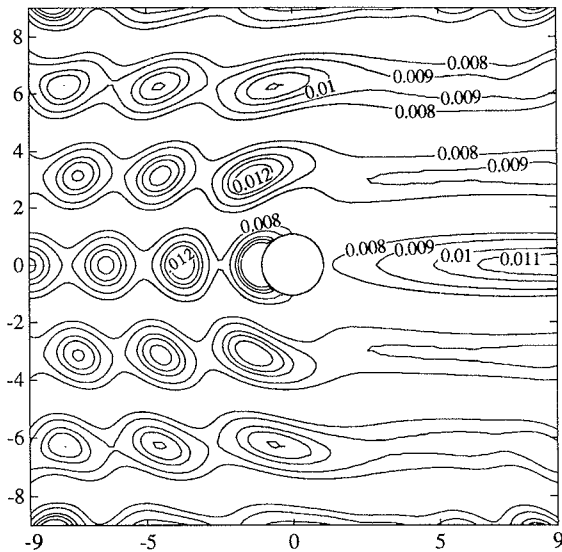

FIG. 14. The curves of equal amplitude (co-amplitude with units in meters) for the incident waves with longitudinal and lateral wave numbers $k_x = 1.0$ m^{-1} and $k_y = 0.5$ m^{-1}, respectively.

FIG. 15. The curves of equal phase (co-phase) for the incident waves with longitudinal and lateral wave numbers $k_x = 1.0$ m^{-1} and $k_y = 0.5$ m^{-1}, respectively.

FIG. 16. The curves of equal amplitude (co-amplitude with units in meters) for the incident waves with longitudinal and lateral wave numbers $k_x = 1.0$ m^{-1} and $k_y = 1.0$ m^{-1}, respectively.
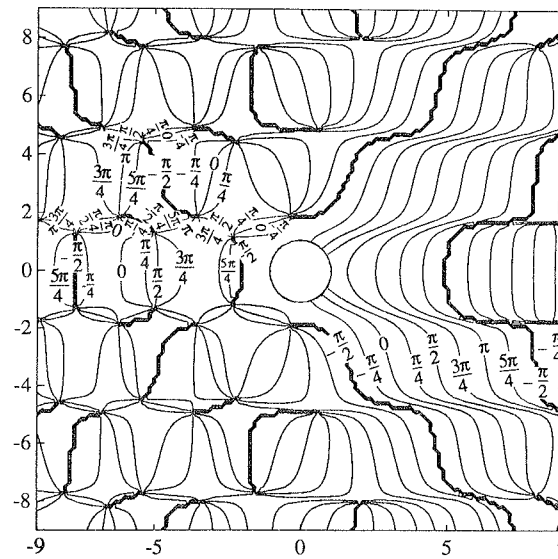
FIG. 17. The curves of equal phase (co-phase) for the incident waves with longitudinal and lateral wave numbers $k_x = 1.0$ m^{-1} and $k_y = 1.0$ m^{-1}, respectively.

lateral wave number becomes larger; a beautiful amphidromic pattern is shown in Fig. 17 when $k_y = 1$ m^{-1}. However, there is always a region behind the cylinder, where there are no amphidromic points; the wave crests appear to be parallel again, at least within some sizeable neighbourhood of a particular spatial point. The waves are therefore no longer "short-crested" in the lee region of the cylinder. This region of absent short-crested waves becomes wider as the wavelength in the lateral direction becomes larger.

5. CONCLUSIONS

An exact solution has been found for the diffraction of short-crested waves incident on a circular cylinder. The wave loads on the cylinder become larger as the incident waves become less short-crested. Inertia and drag coefficients can still be defined; they are constants as long as ka remains the same. However, the total force exerted on a cylinder is linearly proportional to the wave number in the direction of the wave propagation for a constant ka. The run-up and the pressure distribution on the cylinder are quite different from that of plane incident waves; their pattern becomes very complex as ka becomes very large. Amphidromic points formed up for the diffracted short-crested waves. The phases near two adjacent amphidromic points rotate clockwise and counter-clockwise around these amphidromic points, respectively. In the lee region behind the cylinder, wave amplitude generally becomes smaller as the crests of the incident waves become shorter. The short-crested waves also seem to have disappeared in this region.

REFERENCES

BETTESS, P. and ZIENKIEWICZ, O.C. 1976. Diffraction and refraction of surface waves using finite and infinite elements. *Int. J. Num. Meth. Engng* **11**, 1271–1290.

CHAKRABARTI, S.K. and TAM, A. 1975. Interaction of waves with large vertical cylinder. *J. Ship Res.* **19**, 22–33.

FUCHS, R.A. 1952. On the theory of the short-crested oscillatory waves. In *Gravity Waves*, National Bureau of Standards Circular No. 521, pp. 187–200.

HSU, J.R.C., TSUCHIYA, Y. and SILVESTER, R. 1979. Third-order approximation to short-crested waves. *J. Fluid Mech.* **90**, 179–196.

JEFFREYS, H. 1924. On water waves near the coast. *Phil. Mag. ser 6, 17*, 44–48.

MACCAMY, R.C. and FUCHS, R.A. 1954. Wave forces on piles: a diffraction theory. U.S. Army Corps of Engineering, Beach Erosion Board, Technical Memorandum No. 69.

MEI, C.C. 1989. The applied dynamics of ocean surface waves. In *World Scientific,* pp. 315–316.

NEELAMANI, S., SUNDAR, V. and VENDHAN, C.P. 1989. Dynamic pressure distribution on a cylinder due to wave diffraction. *Ocean Engng* **16**, 343–353.

ROBERTS, A.J. 1983. Highly nonlinear short-crested water waves. *J. Fluid Mech.* **135**, 301–321.

SOMMERFELD, D. 1949. *Partial Differential Equations in Physics.* Academic Press, New York.

TSAY, T.-K., ZHU, W. and LIU, P.L.-F. 1989. A finite element model for wave refraction, diffraction, reflection and dissipation. *Appl. Ocean Res.* **11**, 33–38.

WATSON, G.N. 1962. *Theory of Bessel Functions.* Cambridge University Press, Cambridge.

APPENDIX

Following Mei (1989), the inertia and drag coefficients per unit height are related to the total force per unit length as

$$Re\left(\frac{dF_x}{dz}\right) = \rho\pi a^2(C_M\dot{U} + \omega C_D U) \ ,$$

where U is the velocity of the incident waves at $x = 0$ in the absence of the cylinder. The inertia and drag coefficients for the short-crested waves and, C_M and C_D, are thus defined as

$$C_M = -\frac{I}{\pi a^2 k_x} \ ,$$

and

$$C_D = \frac{R}{\pi a^2 k_x} \ ,$$

where R and I are the real and imaginary parts of $\frac{dF_z}{dz}$ without the constant term:

$$\rho g A\,\frac{\cosh k(z+d)}{\cosh kd}\,e^{-i\omega t} \ .$$

After some simplification, the inertia coefficient, C_M, and drag coefficient, C_D, per unit height can be obtained as

$$C_M = \frac{2}{k_x a}\Bigg\{ J_1(k_x a)J_0(k_y a) + \sum_{n=1}^{\infty}(-1)^n[J_{2n+1}(k_x a) - J_{2n-1}(k_x a)]J_{2n}(k_y a)$$

$$-\frac{J_1(ka)J_1'(ka) + Y_1(ka)Y_1'(ka)}{k[J_1'(ka)^2 + Y_1'(ka)^2]}\Bigg[k_x J_1'(k_x a)J_0(k_y a) + k_y J_1(k_x a)J_0'(k_y a)$$

$$+ \sum_{n=1}^{\infty} (-1)^n k_x (J'_{2n+1}(k_x a) - J'_{2n-1}(k_x a)) J_{2n}(k_y a)$$

$$+ \sum_{n=1}^{\infty} (-1)^n k_y (J_{2n+1}(k_x a) - J_{2n-1}(k_x a)) J'_{2n}(k_y a) \Bigg] \Bigg\} ,$$

and

$$C_D = \frac{4}{\pi k (k_x a)(ka)[J'_1(ka)^2 + Y'_1(ka)^2]} \Bigg\{ k_x J'_1(k_x a) J_0(k_y a) + k_y J_1(k_x a) J'_0(k_y a)$$

$$+ \sum_{n=1}^{\infty} (-1)^n [k_x (J'_{2n+1}(k_x a) - J'_{2n-1}(k_x a)) J_{2n}(k_y a)$$

$$+ k_y (J_{2n+1}(k_x a) - J_{2n-1}(k_x a)) J'_{2n}(k_y a)] \Bigg\} .$$